Bioactive Materials 31 (2024) 463–474

Contents lists available at ScienceDirect

Bioactive Materials

journal homepage: www.keaipublishing.com/en/journals/bioactive-materials

Decellularized heart extracellular matrix alleviates activation of hiPSC-derived cardiac fibroblasts

Charles M. Kerr [a], Sophia E. Silver [b], Yi Sun Choi [c], Martha E. Floy [d], Amy D. Bradshaw [f,g], Seung-Woo Cho [c], Sean P. Palecek [d], Ying Mei [b,e,*]

[a] Molecular Cell Biology and Pathobiology, Medical University of South Carolina, Charleston, SC, USA
[b] Bioengineering Department, Clemson University, Clemson, SC, USA
[c] Department of Biotechnology, Yonsei University, Seoul, South Korea
[d] Department of Chemical and Biological Engineering, University of Wisconsin-Madison, Madison, WI, USA
[e] Department of Regenerative Medicine and Cell Biology, Medical University of South Carolina, Charleston, SC, USA
[f] Department of Medicine, Division of Cardiology, Medical University of South Carolina, Charleston, SC, USA
[g] Ralph H. Johnson Veterans Affairs Medical Center, SC, USA

ARTICLE INFO

Keywords:
Activated fibroblast
Biomimetic substrate
Extracellular matrix
hiPSC-derived cardiac fibroblasts
RNA sequencing

ABSTRACT

Human induced pluripotent stem cell derived cardiac fibroblasts (hiPSC-CFs) play a critical role in modeling human cardiovascular diseases *in vitro*. However, current culture substrates used for hiPSC-CF differentiation and expansion, such as Matrigel and tissue culture plastic (TCPs), are tissue mismatched and may provide pathogenic cues. Here, we report that hiPSC-CFs differentiated on Matrigel and expanded on tissue culture plastic (M-TCP-iCFs) exhibit transcriptomic hallmarks of activated fibroblasts limiting their translational potential. To alleviate pathogenic activation of hiPSC-CFs, we utilized decellularized extracellular matrix derived from porcine heart extracellular matrix (HEM) to provide a biomimetic substrate for improving hiPSC-CF phenotypes. We show that hiPSC-CFs differentiated and expanded on HEM (HEM-iCFs) exhibited reduced expression of hallmark activated fibroblast markers versus M-TCP-iCFs while retaining their cardiac fibroblast phenotype. HEM-iCFs also maintained a reduction in expression of hallmark genes associated with pathogenic fibroblasts when seeded onto TCPs. Further, HEM-iCFs more homogenously integrated into an hiPSC-derived cardiac organoid model, resulting in improved cardiomyocyte sarcomere development. In conclusion, HEM provides an improved substrate for the differentiation and propagation of hiPSC-CFs for disease modeling.

1. Introduction

Cardiovascular disease remains the leading cause of mortality death worldwide [1]. Alterations in the extracellular matrix (ECM) are key events in cardiovascular disease and are often used as predictors of mortality and disease progression [2–4]. The cardiac ECM is made up of collagens, growth factors, proteoglycans, and glycoproteins that are dynamically remodeled by cardiac fibroblasts (CFs) during development, homeostasis, and cardiovascular disease [5]. CF mediated pathogenic remodeling of the ECM (i.e., fibrosis) has been linked to various cardiovascular diseases and can ultimately lead to heart failure [6,7]. In addition, the lack of major subsets of fibroblasts during development leads to disrupted healing responses during injury and can result in cardiac rupture [8]. Notably, the structure and composition of cardiac ECM can influence cardiac fibroblast behavior. For example, decellularized ECM derived from dilated cardiomyopathy biopsies triggered pathogenic activation of cardiac fibroblasts *in vitro* [9]. This highlights the intricate communication between fibroblasts and ECM in cardiac pathology.

The current *in vitro* cardiovascular disease models typically are insufficient with recapitulating the cardiac ECM and fibroblast interactions, with previous models emphasizing the use of human induced pluripotent stem cell derived cardiomyocytes (hiPSC-CMs) on 2D substrates [10–13]. More recent studies combine hiPSC-CMs with supporting cell types (e.g., hiPSC-CFs) to fabricate multicellular engineered

Peer review under responsibility of KeAi Communications Co., Ltd.
* Corresponding author. Bioengineering Department, Clemson University, Clemson, SC, USA.
E-mail addresses: kerr.charlesm@gmail.com (C.M. Kerr), sesilve@g.clemson.edu (S.E. Silver), yisunchoi@gmail.com (Y.S. Choi), mfloy753@gmail.com (M.E. Floy), bradshad@musc.edu (A.D. Bradshaw), seungwoocho@yonsei.ac.kr (S.-W. Cho), sppalecek@wisc.edu (S.P. Palecek), mei@clemson.edu (Y. Mei).

https://doi.org/10.1016/j.bioactmat.2023.08.023
Received 12 April 2023; Received in revised form 1 August 2023; Accepted 30 August 2023
Available online 7 September 2023

Abbreviations

DCM-CF	dilated cardiomyopathy-cardiac fibroblasts; cardiac fibroblasts derived from donors experiencing dilated cardiomyopathy
ECM	xtracellular matrix
Healthy-CF	healthy cardiac fibroblasts; cardiac fibroblasts isolated from healthy human donors
HEM	heart ECM; pepsin digested porcine heart ECM
HEM-iCF	hiPSC-CF differentiated and expanded on HEM-coated TCP
hiPSC	human induced pluripotent stem cells
hiPSC-CF	hiPSC-derived cardiac fibroblasts
hiPSC-CM	hiPSC-derived cardiomyocytes
hiPSC-EC	hiPSC-derived endothelial cells
M-TCP-iCF	hiPSC-CF differentiated on Matrigel and expanded on TCP
MAT	Matrigel
TCP	tissue culture plastic

3D cardiac microtissues [14–16]. Presently, hiPSC-CFs have been differentiated on Matrigel and expanded on tissue culture plastic (TCP). Derived from Engelbreth-Holm-Swarm tumors in mice, Matrigel is composed of vast array of ECM proteins that does not necessarily reflect those in cardiac ECM [17]. In addition, TCPs have been well known to stimulate fibroblast activation [18]. Meanwhile, decellularized cardiac ECM scaffolds and gels are promising in vivo therapeutics for treating heart disease [19–22] while also demonstrating benefits for enhancing cardiac phenotypes during hiPSC-CM differentiations in 2D cultures as a solubilized TCP coating [23–25]. Thus, we reasoned the utilization of a biomimetic substrate of healthy ECM would better foster homeostatic hiPSC-cardiac fibroblasts for downstream applications.

Here, we report for the first time, using heart ECM derived from porcine hearts (HEM) as a biomimetic substrate to enhance hiPSC-CF differentiation and expansion through a reduction in activation potential of TCP. Initially, we show that hiPSC-CFs, differentiated on Matrigel and expanded on tissue culture plastic (TCP) (M-TCP-iCFs) transcriptomically align with activated fibroblasts found within dilated cardiomyopathy patients and even exhibit heightened enrichment for activated fibroblast properties. Additionally, we show that HEM does not adversely alter hiPSC-CFs' cardiac fibroblast phenotype while limiting the activation of hiPSC-CF during differentiation. hiPSC-CFs differentiated on HEM (HEM-iCFs) also maintained their inactivation during expansion on HEM. Further activation of M-TCP-iCFs was reduced when plated onto HEM. In an isogenic cardiac organoid model, HEM-iCFs more homogeneously integrated within an isogenic cardiac organoid model, improved α-sarcomeric actinin expression in hiPSC-CMs and reduced the angiogenic properties of hiPSC-endothelial cells (hiPSC-EC). In conclusion, this study demonstrates that biomimetic ECM substrates can enhance cardiac fibroblast differentiation and expansion to develop high fidelity multicellular cardiac tissues for disease modeling.

2. Methods

2.1. RNA-sequencing meta-analysis

Raw FASTQ files were retrieved from the European Nucleotide archive (https://www.ebi.ac.uk/) using the accession numbers for DCM and healthy primary cardiac fibroblasts (PRJNA649946/GSE155495 [9]) and hiPSC-derived cardiac cell types (PRJNA707062/GSE168380 [26] and PRJNA328021\ GSE84085 [27]). Genome alignment was performed using RNA STAR (v2.7.8a) in the Galaxy Project online platform (v21.01, https://galaxyproject.org/). Reads were aligned to the hg38 reference genome GRCh38.p13 built into RNA STAR. Gene counts were subsequently generated using htseq-count (v13.5). The next stage of analyzes were then performed in R Studio (v1.3.1093) (R language v3.6.1).

Initially, we examined the impact of pooling samples across several studies utilizing principal component analysis (PCA). Our initial assessment identified distinct differences between primary and hiPSC derived cell type across the 3 studies (Supplementary Fig. 1). These studies also contained samples from human primary and hPSC derived epicardial cells and cardiomyocytes as well as hiPSC second heart field derived fibroblasts [26]. To provide stronger confidence in the underlying transcriptomic differences between primary and hiPSC-derived cardiac fibroblasts, we perform batch correction using "ComBat_seq" [28] in the Surrogate Variable Analysis ("sva", v3.35.2) R package. After batch correction, samples from DCM-CFs, Healthy-CFs and hiPSC-CFs were used for our subsequent analysis.

Principal Component Analysis (PCA) and gene set enrichment analysis (GSEA) was performed as previously reported using the Bioconductor (v3.1.2) [29,30] package in R Studio [31,32]. Briefly, a gene count matrix generated from the htse-count package on GalaxyProject was loaded into R Studio. Genes with <2 counts were removed. The package "DESeq2" (v1.32) [33] was used to create a summarized experiment object from the gene counts matrix. For PCA analysis, an r-log transformation was performed on the summarized experiment object to stabilize the variation and the subsequent PCA analysis was performed using the "prcomp" function. PCA plots were generated using the package "ggplot2" (v3.3.5) [34]. Gene loadings for PC1 and PC2 were used as gene rankings for GSEA (v4.0.3) (Broad Institute) [35,36]. GSEA was performed using a curation of canonical pathway databases composed of databases: BioCarta, KEGG, Pathway Interaction Database, Reactome, SigmaAldrich, Signaling Gateway, SuperArray SABiosciences and Wikipathways, (C2.all.v2022.1.Hs.symbols.gmt; http://www.gsea-msigdb.org/gsea/msigdb/human/collection_details.jsp#C2) (19 October 2022). The R package, "DESeq2" [33], was used to perform the differential gene expression (DGE) analysis. Three DGE analysis were performed: 1) DCM-CF vs. Healthy-CF, 2) hiPSC-CF vs. Healthy-CF, and 3) DCM-CF vs. hiPSC-CF. Volcano plots were generated using "ggplot2". DEG's that exhibited a log2fold change greater than 1.33 (Fold Change >2.5) or less than 1.33 (Fold change < -2.5) and an adjusted p-value <0.001 were loaded into Metascape [37].(https://metascape.org/), an online tool for pathway overrepresentation analysis. All canonical pathway databases were used in the pathway analysis and visualized used "ggplot2". Gene Set Variation Analysis (GSVA) was performed using the R package, "gsva", comparing DC-CF, Healthy-CF and hiPSC-CF to defined gene sets generated from a single cell sequencing study examining the populations of cells sequence from healthy and DCM hearts of human donors [38]. We used the top genes that defined the clusters "Activated Fibroblast", "Fibroblast I" and "Fibroblast II" to be used for comparing the gene enrichment of the different cardiac fibroblasts in these cell type clusters.

2.2. HEM decellularization, digestion and cell culture plastic coating

HEM was produced based on previously established methods [39]. Briefly, samples of left ventricular tissues were isolated from whole porcine hearts purchased locally. Left ventricular tissues were cleaned of adipose tissue and blot clots and cut into smaller pieces. The tissues were decellularized using a serial treatment of 1% (v/v) SDS (Sigma-Aldrich, St. Louis, MO USA) for 24 h and then with 1% (w/v) Triton X-100 (Sigma-Aldrich, St. Louis, MO USA) supplemented with 0.1% (v/v) ammonium hydroxide (Sigma-Aldrich, St. Louis, MO USA) for 6 h at 4 °C under agitation. The decellularized tissues were rinsed with distilled water for 24 h, treated with 1% (v/v) penicillin-streptomycin (Thermo Fisher Scientific, Waltham, MA, USA) for 2 h and then rinsed again with distilled water. The decellularized HEM was lyophilized and stored at

4 °C. The decellularized HEM was cut into smaller pieces and dissolved as 10 mg of tissue per 1 mL in a pepsin solution (4 mg/mL pepsin in0.02 M HCl) (Roche Life Sciences, Penzberg, DE) for 48 h at room temperature with constant stirring. The HEM solution was aliquoted and stored at −20 °C for no more than 3 months. For coating TCP, the HEM solution (10 mg/mL) was diluted in 0.02 M acetic acid to 20 μg/mL and added to TCP wells. The plates were incubated for >16 h at 37 °C, 5% CO_2. Immediately prior to seeding cells, the HEM solution was aspirated, and the wells were rinsed with 1X DPBS (Thermo Fisher Scientific, Waltham, MA).

2.3. hiPSC (19-9-11) expansion and maintenance

Prior to hiPSC thawing, TCP was coated with hESC-certified Matrigel (Corning Inc., Corning, NY, USA) for >16 h at 37 °C, 5% CO_2 using the manufacturer's recommended dilution factor. The hiPSC cell line, 19-9-11 (WiCell, Madison, WI, USA), were gently thawed and resuspended in mTeSR1 media (StemCell Technologies, Vancouver, Canada) and centrifuged (200×*g*, 5 min, room temperature). The cells were resuspended in mTeSR1 with 5 μM Y-27632 (Tocris Bioscience, Bristol, UK) and seeded onto Matrigel-coated wells of TCPs. The hiPSCs were

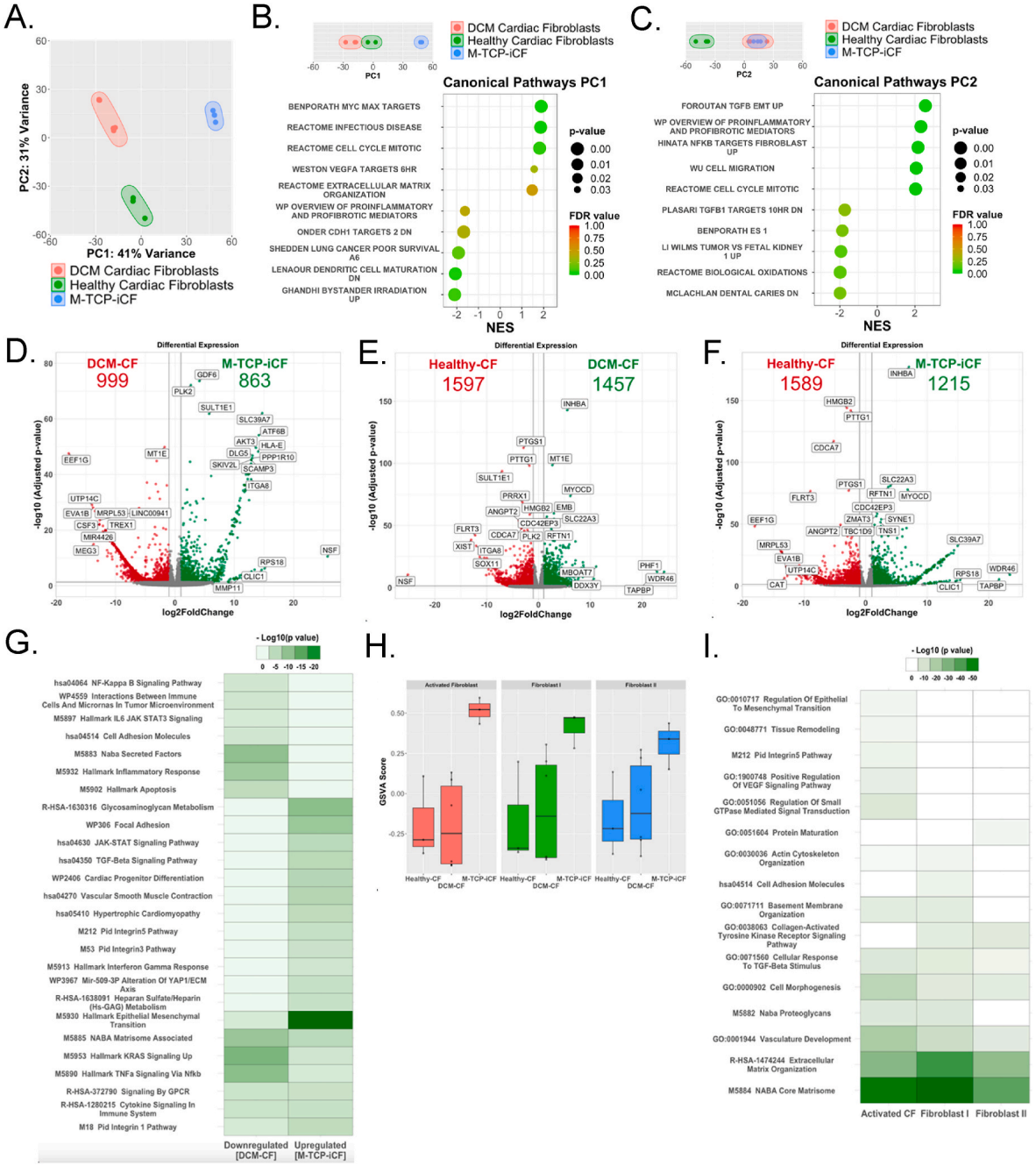

Fig. 1. M-TCP-iCF display an enhanced activated fibroblast associated transcriptome

(A) Principal component analysis of DCM-CF (n = 6), Healthy-CF (n = 3), and M-TCP-iCF (n = 3) differentiated on Matrigel and expanded on tissue culture plastic. (B) GSEA using enrichment of canonical pathways (C2.all.v2022.1.Hs.symbols.gmt) on gene loadings of PC1 and PC2 (C). Volcano plot of differentially expressed comparing M-TCP-iCF vs. DCM-CF (D), DECM-CF vs. Healthy-CF (E), and M-TCP-iCF vs. Healthy-CF (F). Genes were considered significant if adjusted p-value >0.001 and |log2fold| > 1.33. (G) Pathway overrepresentation analysis of upregulated and downregulated genes comparing M-TCP-iCF vs. DCM-CF. (H) GSVA analysis utilizing genelists of scRNA-seq clusters of DCM and healthy hearts of Activated Fibroblasts, Fibroblast I and Fibroblast II and reference gene sets(Chaffin et al., 2022). (I) Pathway analysis of DCM and healthy hearts scRNA-seq-derived gene sets.

maintained at 37 °C, 5% CO_2 and medium was exchanged daily within 27 h. Once 90% confluent, hiPSCs were passaged using Versene (Thermo Fisher Scientific) (5 min, 37 °C, 5% CO_2). Versene was aspirated and hiPSCs were gently rinsed off the wells with mTeSR1 and collected. Cells were replated 1:6 on fresh Matrigel-coated TCP. hiPSC were passaged 4 times prior to beginning all differentiations.

2.4. hiPSC-cardiac fibroblast differentiation

hiPSC-CF were differentiated based on previous methods [26] from the 19-9-11 hiPSC stem cell line. In summary, hiPSCs were differentiated based on the GiWi protocol to derived cardiac progenitors [40], differentiated into hiPSC-epicardial cells [27,41]and then subsequently differentiated into hiPSC-CF. For cardiac progenitor differentiation, 90% confluent hiPSC were singularized using Accutase (Sigma-Aldrich) (6 min, 37 °C, 5% CO_2) and seeded onto Matrigel-coated TCP at 300,000 cells/cm^2 in mTeSR1 with 5 μM Y-27632 (Day −2). Media was exchanged 24 h later. On Day 0, cells were treated with 6 μM CHIR99021 (Selleck Chemicals, Houston, TX, USA) in RPMI 1640 (Thermo Fisher Scientific) supplemented with B27 Minus Insulin (Thermo Fisher Scientific) (RPMI/B27$^-$) for precisely 24-h after which media was replaced with fresh RPMI/B27$^-$. On Day 3, cells were treated for precisely 48 h with IWP2 (Sigma-Aldrich) in RPMI/B27$^-$ after which media was exchanged. By Day 6, these cells are considered to be cardiac progenitors. For hiPSC-epicardial differentiation, Day 6 cardiac progenitors were dissociated using Accutase (10 min, 37 °C, 5% CO_2) and replated 50,000 cells/cm^2 in LaSR basal media composed of Advanced DMEM/F12 (Thermo Fisher Scientific), 10 μg/mL L-Ascorbic Acid (Sigma-Aldrich) and 1X GlutaMAX (Thermo Fisher Scientific) and further supplemented with 5 μM Y-27632. On Day 7, cells were treated for 48 h with 8 μM CHIR99021 in LaSR; after 24 h, fresh LaSR with CHIR99021 was exchanged. After the 48-h treatment, the media was exchanged daily with LaSR basal until Day 12. On Day 12, cells were considered to be hiPSC-epicardial and passaged 1:6 and/or cryopreserved in LaSR supplemented with 0.5 μM A83-01 (Abcam, Cambridge, UK), 10% FBS (Sigma Aldrich), and 10% DMSO (Sigma-Aldrich). For downstream applications, hiPSC-epicardial cells were thawed in LaSR supplemented with 10% FBS, 0.5 μM A83-01 and 5 μM Y-27632 on Matrigel-coated TCP. hiPSC-epicardial cells were maintained in LaSR supplemented with 0.5 μM A83-01 (37 °C, 5% CO_2) and passaged 2–3 times prior to hiPSC-CF differentiation. hiPSC-Epicardial cells were passaged at 90% confluency using TrypLE (10 min, 37 °C, 5% CO_2) and replated in LaSR supplemented with 0.5 μM A83-01and 5 μM Y-27632 onto Matrigel-coated TCP. hiPSC-CF differentiation (Fig. 2B) started once hiPSC-epicardial cells reached 100% confluency on Matrigel-coated TCP. The hiPSC-epicardial cells were passaged 1:1 onto either Matrigel- or HEM-coated TCP (Day −1). hiPSC-CF differentiation began on Day 0 with 10 days of treatment with LaSR +10 ng/mL βFGF (Invitrogen, Waltham, MA, USA) and media was changed daily. On Day 10, cells were considered to be hiPSC-CF and passaged onto either uncoated TCP or HEM-coated TCP in FibroGRO Complete Media (Millipore Sigma, Burlington, MA, USA) with 2% FBS and 1X GlutaMAX. Cells were maintained in FibroGRO and passaged 1:6 using TrypLE when they reached 80–90% confluency.

2.5. mRNA isolation, cDNA synthesis and RT-qPCR analysis

For Real Time-quantitative Polymerase Chain Reaction (RT-qPCR) analysis, mRNA was isolated using the E.N.Z.A. Total RNA Isolation kit I (Omega Bio-Tek, Norcross, GA, USA) according to the manufacturer's instructions. Briefly, hiPSC-CFs were lysed using TRK Lysis buffer supplemented with 1:1000 dilution of β-mercaptoethanol(Sigma-Aldrich). Solutions of lysed cells were homogenized using the Omega Homogenizer spin columns. Following homogenization, mRNA was bound to HiBind mRNA binding columns and rinsed once with Wash Buffer I and twice with Wash Buffer II. mRNA was eluted in RNAse-, DNAse-Free DI water (Thermo Fisher Scientific) and measured using a NanoDrop One Microvolume UV–Vis Spectrophotometer (Thermo Fisher Scientific). For cDNA synthesis, the iScript cDNA synthesis kit (Bio-Rad, Hercules, CA, USA) was used according to the manufacturer's instructions using an Axygen MacGENE II Thermocycler (Thermo Fisher Scientific). Real Time-qPCR was performed using the Life Technologies Taqman probe system. 25 ng of cDNA templates were mixed with 2X Applied Biosystems Universal PCR Mastermix (Thermo Fisher Scientific) and Taqman primers and probes (shown below) (Thermo Fisher Scientific) according to the manufacturer's instructions and ran on CFX96 Real Time PCR detection machines (Bio-Rad). mRNA expression per gene was expressed as 2^{-ddCt}. First, data was normalized as the difference in cycle threshold (Ct) of the gene of interest to the housekeeping gene, GAPDH, (ΔCt) and then normalized per experimental group by taking the difference in ΔCt of the sample of interest to the negative control(ΔΔCt) and reported as the mRNA relative expression ($2^{-\Delta\Delta Ct}$).

Gene	Taqman Assay ID
GAPDH	Hs_02786624_g1
ACTA2	Hs_00426835_g1
COL1A1	Hs_001164004_m1
TGFB1	Hs_0098133_m1

2.6. Flow cytometry analysis

To prepare cells for flow cytometry, hiPSC-CF were dissociated using 1X TrypLE select (Thermo Fisher Scientific) for 10 min. Cells were centrifuged (200×*g*, 5 min, room temperature) and resuspended in cold 1% Paraformaldehyde for fixation (20 min, 4 °C). Cells were diluted 1:10 with 1X PBS and centrifuged (200×*g*, 5 min, room temperature). Cells were then rinsed once with Flow Buffer (1X DPBS, 1% Bovine Serum Albumin (Thermo Fisher Scientific) and 0.1% Triton X-100 (Sigma-Aldrich)) and stored at 4 °C. Fixed cells were then centrifuged (200×*g*, 5 min, room temperature) and resuspended in Flow Buffer with Rabbit anti-Vimentin primary antibody (1:200) (abcam). An unstained control group was incubated in only Flow Buffer. Cells were incubated with primary antibody or Flow Buffer overnight at 4 °C. Post-incubation, all groups were rinsed with Flow Buffer, centrifuged (200×*g*, 5 min, room temperature) and resuspended in Flow Buffer with Goat anti-Rabbit Alexa Fluor 647 secondary antibody (abcam) and incubated for 1 h at room temperature, protected from light. Stained cells were rinsed twice, and flow cytometry analysis was performed using a MACSQuant Analyzer 10 (Miltenyi Biotec) and analysis performed using FlowJo (FlowJo, Ashland, OR, USA).

2.7. 2D fluorescent imaging and quantification

hiPSC-CF were seeded at 5000 cells/cm^2 and fixed 2 days post-seeding with 4% Paraformaldehyde (20 min, room temperature). Cells were rinsed with 1X DPBS + Ca^{2+} + Mg^{2+} (Thermo Fisher Scientific) twice and stored in 1X DPBS + Ca^{2+} + Mg^{2+} at 4 °C. Antigen blocking was performed using 10% Goat Serum (Millipore Sigma) in PBST1 (1X DPBS + Ca^{2+} + Mg^{2+} supplemented with 0.01% Triton-X) (Sigma Alrich) (1 h, room temperature) and then rinsed twice with PBST1. Cells were then stained with primary antibodies (Rabbit anti-Vimentin (1:200), Mouse anti-CD90 (1:200) (Thermo Fisher Scientific) or Rabbit anti-α-Smooth Muscle Actin (1:100) (abclonal, Wuhan, Hubei, CN) in PBST1 (>16 h, 4 °C). Cells were rinsed twice with PBST1 and stained with secondary antibodies (Goat anti-Rabbit Alexa Fluor 647 (Abcam) (1:200), Goat anti-Mouse Alexa Fluor 488 (Abcam) (1:200)) (1 h, room temperature, protected from light). Stained cells were rinsed once with PBST and then stained with NucBlue nuclei stain (Thermo Fisher Scientific) diluted in PBST1 according to the manufacturer's instruction (20 min, room temperature, protected from light). Cells were rinsed twice with PBST1 and then a circular coverslip was mounted on top of

cells within well of TCP plates using Fluoroshield(Sigma-Aldrich). Images were taken using a BZ-X All-in-One Fluorescence Microscope (Keyence, Osaka, JP) using the same excitation and parameters for each image. Analysis of images were performed using FIJI (National Institute of Health). For measuring area of fluorescence of CD90, Vimentin and αSMA, image threshold was performed on 8-bit images of each channel to measure the total area of fluorescent channel. Using the Nuclei channel, the number of cells per image were calculated and used to divide the fluorescent area by the number of cells per field of view (FOV).

2.8. Collagen contraction assay

M-TCP-iCF and HEM-iCF were first dissociated using TrypLE select (10 min, 37 °C, 5% CO_2). Cells were quenched with FibroGRO and centrifuged (200×*g*, 5 min, room temperature). Cells were resuspended to 3 million cells/mL in cold FibroGRO and kept on ice. Solutions of rat tail Collagen Type I (collagen I) (Corning) and suspended hiPSC-CF cells were prepared on ice with final concentrations of 1.75 mg/mL collagen I and 600,000 hiPSC-CFs/mL. Ensuring collagen gel suspensions remain cold, 500 mL of gel suspension were added to individual wells of a 24-well plate and allowed to gel for 16 h at 37 °C, 5% CO_2. After the incubation, the gels were carefully detached from the walls of the wells using a 10 μL pipet tip. After 48 h, images were taken of the gels and Fiji imaging software was used to measure the area of the gel per well.

2.9. hiPSC-CF spheroid analysis

hiPSC-CF spheroids were fabricated based on previously established methods [42–44]. Agarose molds containing micro-recesses for 3D spheroid self-assembly were fabricated with 2% agarose, 24-h prior to seeding. Molds were maintained in FibroGRO media to prevent drying. Both M-TCP-iCF and HEM-iCF were dissociated using TrypLE and resuspended to 4×10^6 cells/mL and 80 μL of each cell type were loaded into a well of an agarose mold. Cells were allowed to settle to the bottom of micro recesses for 20 min then 2 mL of FibroGRO were carefully added to wells surrounding molds to prevent washing out the cells. Two days after spheroid fabrication, images of spheroids were taken and spheroids were lysed for downstream RT-qPCR (see Methods 2.5). Images of spheroids were used to quantify spheroid area in FIJI.

2.10. Isogenic organoid fabrication and hiPSC-CM and hiPSC-EC differentiation

For isogenic organoid fabrication, hiPSC-CM and hiPSC-EC differentiations were performed in addition to hiPSC-CF. The hiPSC-CM differentiation was based on previously established methods [26,40]. Briefly, Day 6 hiPSC cardiac progenitors (see Methods 2.4) were differentiated after seeding 19-9-11 hiPSC on Day −2 at 550,000 cells/cm^2 into a Matrigel-coated 48-well plate and treated with 8–9 μM CHIR99021 on Day 0. On Day 7, media was exchanged for RPMI 1640 supplemented with B27 with Insulin (Thermo Fisher Scientific) (RPMI/B27$^+$) and media was replaced every other day. On Day 10, cells were purified for 48-h using lactate purification [45] consisting of feeding cells with glucose free DMEM (Thermo Fisher Scientific) supplemented with 4 mM Na-L-Lactate (BeanTown Chemical, Hudson, NH, USA). Cells were allowed to recover for 2 days after which they were prepared for cryopreservation (Day 14) [46]. On Day 14, purified hiPSC-CM were dissociated using Accutase (37 °C, 5% CO_2, 40 min), quenched with RPMI/B27$^+$, centrifuged (200×*g*, 5 min, room temperature), and resuspended in RPMI/B27$^+$ supplemented with 30% Defined FBS (Cytiva Life Sciences, Marlborough, MA, USA) and 10% DMSO (Sigma-Aldrich). hiPSC-CM were frozen overnight at −80 °C in a Nalgene Mr. Frosty Freezing Container (Thermo Fisher Scientific) and then transferred to Liquid Nitrogen for long term storage. Cryopreserved hiPSC-CM were thawed and seeded onto Matrigel-coated plates at 8500 cells/cm^2 in RPMI/B27$^+$ supplemented with 10 μM Y-27632. After 24-h, hiPSC-CM expansion was initiated [46,47] and media was replaced with RPMI/B27$^+$ supplemented with 4 μM CHIR99021. Media was exchanged every other day for 2 weeks until cardiac organoid fabrication.

hiPSC-EC differentiation was based on previous reports [48–50]. Briefly, 80–90% confluent 19-9-11 hiPSC's were dissociated with Accutase (6 min, 37 °C, 5% CO_2) quenched with equal parts mTeSR1 and centrifuged (200×*g*, 5 min, room temperature). Cells were resuspended in mTeSR1 supplemented with 5 μM Y-27632 and seeded 125,000 cells/cm^2 (Day-2) and media was replaced with mTeSR1, 1 day after seeding (D-1). On Day 0, cells were treated with 6 μM CHIR99021 in LaSR Basal for precisely 48 h, replacing with fresh treatment media after 24 h. On Day 2, media was changed to LaSR Basal and replaced daily. On Day 5, cells were dissociated with Accutase (10 min, 37 °C, 5% CO_2) quenched with LaSR Basal and purified using CD34$^+$ Microbeads (Miltenyi Biotec) following the manufacturer's instructions. Purified CD34$^+$ cells were seeded 10,000/cm^2 onto collagen I-coated TCP (50 μg/mL) in Endothelial Growth Media-2 (EGM2) (PromoCell, Heidellberg, DEU) supplemented with 0.5 μM A83-01 and 10 μM Y-27632. Media was replaced 1 day after with EGM2 supplemented with 0.5 μM A83-01 (Day 6) and media was further exchanged every other day. On Day 10, cells were purified by treatment with Versene for 5 min to remove non-endothelial cells and rinsed with 1X DPBS. Cells were subsequently replated 1:3 onto fresh collagen I-coated plates after dissociation with TrypLE (15 min, 37 °C, 5% CO_2) and maintained in EGM2 supplemented with 0.5 μM A83-01 until cardiac organoid fabrication.

Isogenic cardiac organoid fabrication is based on our previously established methods [31,32,51–53]. Briefly, hiPSC-CM were expanded until confluency and permitted to recover in RPMI/B27$^+$ for 24 h. Agarose molds containing micro-recesses for organoid self-assembly were fabricated with 2% agarose, 24-h prior to seeding. Agarose molds were maintained in organoid media to prevent drying. Organoid media consisted of 48% % RPMI 1640 (Thermo Fisher Scientific), 5.4% Defined FBS, 0.54% Non-essential amino acids (Thermo Fisher Scientific), 30% Fibroblast Growth Media 3 (PromoCell), and 16% EGM2. All cell types were dissociated using TrypLE (37 °C, 5% CO_2): 40 min for hiPSC-CM, 20 min for hiPSC-EC and 10 min for hiPSC-CF. Cells were quenched and collected in their cell-type specific maintenance media, centrifuged (200×*g*, 5 min, room temperature) and resuspended to 5.25×10^6 cells/mL in organoid media. The cells were mixed at the ratio of 70:15:15 (hiPSC-CM: hiPSC-CF: hiPSC-EC); separate organoids with M-TCP-iCF or HEM-iCF were fabricated. Media was aspirated from the agarose mold and 80 μL of mixed cell suspension were added to the wells of the agarose molds. Cells were permitted to settle into the micro-recesses of the agarose molds for 20 min, the wells of the plates were then filled with organoid media and then the organoids were maintained at 37 °C, 5% CO_2. Organoid media was exchanged every other day for 10 days.

2.11. Organoid immunofluorescent staining and analysis

Organoid immunofluorescent staining was performed as previously described [31]. In brief, one well of organoids were embedded in Optimal Cutting Temperature Compound (OCT) (Thermo Fisher Scientific) in Tissue-Tek plastic cryomolds (Sakura Finetek, Torrance, CA, USA), and immediately frozen to −80 °C. Embedded blocks were sectioned using a Cryostat Microtome (Leica Biosystems, Wetzlar, DEU), sections were mounted on glass slides (Fisher Scientific, Pittsburgh, PA, USA) and mounted sections were stored at −20 °C. Sections were then fixed with 100% cold Acetone (12 min) and allowed to dry. Sections were blocked with 10% Goat Serum in 1X DPBS with 0.01% Triton X-100 (PBST2) (1 h, room temperature). Subsequently, sections were stained with primary antibodies (Rabbit anti-α-sarcomeric actinin (αSA) (abclonal) (1:200), Mouse anti-Vimentin (Abcam) (1:200) or Mouse anti-CD31 (BD Pharmigen, San Diego, CA, USA) (1:50)) diluted in PBST2

(>16 h, 4 °C). Sections were then rinsed for 5 min with PBST2 and then stained with secondary antibodies (Goat anti-Rabbit Alexa Fluor 647 (Abcam) (1:200), Goat anti-Mouse Alexa Fluor 488 (Abcam) (1:200)) (1 h, room temperature, protected from light). Sections were then rinsed for 5 min with PBST2 and then stained NucBlue (20 min, room temperature, protected from light). Sections were then rinsed for 5 min with PBST2, twice, and then a coverslip was mounted using Fluoroshield. Sections were imaged using Leica SP5 Confocal microscope (Leica Biosystems). Image analysis was performed in Fiji and the area measurement analysis was performed as outlined in section 2.6. The area of αSA, Vimentin and CD31 was normalized to the area of individual organoids fixed on Day 10 or Day 14, post-organoid fabrication. Vimentin radial analysis was performed as previously described [31] using the Radial Profile plugin in Fiji of vimentin expression.

2.12. Organoid contraction analysis

Cardiac organoid contraction analysis was performed as previously described [31]. Videos of beating organoids were recorded using a Carl Zeiss Axiovert A1 Inverted Microscope and Zen 2011 software (Zeiss). To measure changes in area during contraction and relaxation, a threshold was applied to high contraction videos of contracting organoids and the area of the organoids was subsequently measured for each frame of the video. The changes in area during contraction and relaxation were measured as a percent change in fractional area change amplitude.

2.13. Statistical analysis

Statistical differences between experimental groups were analyzed using GraphPad Prism Statistical tools (v9.3.0) (Dotmatics, Boston, MA, USA). Statistical analysis was performed using one-way ANOVA with post hoc Tukey's multiple comparison's test and Student's t-test; p-value <0.05 was considered significantly different, unless noted. Grub's outlier analysis performed using alpha of 0.1. More specific details regarding each analysis are indicated in figure legends.

3. Results and discussion

3.1. M-TCP-iCFs displayed activated cardiac fibroblast transcriptome

Previous studies have demonstrated M-TCP-iCFs, which are hiPSC-CFs differentiated from epicardial cells on Matrigel and then expanded on TCPs, recapitulate the cardiac fibroblast phenotype when compared to primary cardiac fibroblasts [26]. However, Matrigel is not cardiac specific, and TCP is a well-documented inducer of fibroblast activation. To investigate whether Matrigel and TCP induce activation of hiPSC-CFs, we performed an RNA-sequencing meta-analysis of M-TCP-iCFs [26] and human primary cardiac fibroblasts isolated from healthy (healthy-CFs) and dilated cardiomyopathic hearts (DCM-CFs) [9]. Our samples were batch corrected for inherent differences between hiPSC and primary cell types (see Methods 2.1). Principal component analysis (PCA) revealed that M-TCP-iCFs, healthy-CFs, and DCM-CFs each displayed a unique transcriptome (Fig. 1A). Along Principal Component 1 (PC1), accounting for 41% of the variance, M-TCP-iCFs displayed a unique transcriptome apart from both healthy-CFs and DCM-CFs, suggesting distinct gene expression from primary cardiac fibroblasts. Previous reports have shown slight transcriptomic dissimilarity of hiPSC-cardiac fibroblasts to primary CF [26,54,55], yet hiPSC-CF are more similar to primary CF compared to dermal fibroblasts [26,54]. While our analysis removed general confounding differences between hiPSC and primary cell types, there appeared to remain underlying transcriptomic differences between hiPSC and primary CF. To deduce functional characteristics corresponding to the transcriptomic differences shown in the PCA, gene Set Enrichment Analysis (GSEA) on the gene loadings of PC1 revealed that the M-TCP-iCFs (i.e., positive enrichment) were enriched in "Reactome Cell Cycle Mitotic", "Weston VEGFA targets 6hr", and "Reactome Extracellular Matrix Organization" (Fig. 1B). These pathways are consistent with established reports that activated fibroblasts are more proliferative, angiogenic and capable of remodeling ECM [7]. Further, "Benporath MYC max targets" exhibited the largest significance suggesting enhanced MYC activity, which has been shown to induce activation of renal fibroblasts through integrin and TGFβ signaling [56]. Previous reports have indicated enhanced integrin expression in cells cultured on TCP compared to basement membrane coated TCP [57], and integrin regulation of MYC expression [58]. Together, these results suggested that the cell culture conditions might play a significant role in the activation of the M-TCP-iCFs involving MYC signaling. Additionally, M-TCP-iCFs and DCM-CFs overlapped along PC2 (Fig. 1C) and were enriched in "Overview of Proinflammatory and Profibrotic mediators", "Foroutan TGFB EMT Up", "Hinata NFKB Targets fibroblast up", "Wu cell migration", "Reactome Cell cycle mitotic", also consistent with functions of activated fibroblast. These enriched pathways highlight that M-TCP-iCFs share some pathogenic traits of DCM-CF, but also display enhanced proliferation, VEGF signaling and ECM deposition in comparison to both DCM-CFs and healthy-CFs (Fig. 1B). A complete list of enriched terms for PC1 and PC2 can be found in Supplementary Tables 1 and 2

To further deduce transcriptomic differences between M-TCP-iCFs, healthy-CFs and DCM-CFs, we conducted a differential gene expression (DGE) analysis performing 3 comparisons: 1) M-TCP-iCFs vs. Healthy-CFs, 2) DCM-CFs vs. Healthy-CFs and 3) M-TCP-iCFs vs. DCM-CF. We identified that M-TCP-iCFs and DCM-CFs displayed the most similarity among the DGE comparisons as fewer differentially expressed genes were found between them (Fig. 1D), rather than when each were compared to Healthy-CFs (Fig. 1E and F). Over representation analyses performed using the differentially expressed genes revealed that genes downregulated in M-TCP-iCFs compared to DCM-CFs exhibit higher enrichment in "hallmark inflammatory response" and "NABA matrisome associated", indicating different exposure to pathological stimuli. Meanwhile, M-TCP-iCFs had transcriptomic upregulation associated with the activated fibroblast phenotype, such as "hsa04350 TGF-beta Signaling Pathway" (Fig. 1G). As bulk RNA-sequencing of isolating CFs from heart tissue may contain a heterogenous population of fibroblasts, we performed a Gene Set Variation Analysis (GSVA) using cell-type specific gene lists derived from single cell RNA-sequencing data of healthy and DCM donors [38] to identify the similarity of M-TCP-CFs to a homogenous, activated fibroblast population. The M-TCP-iCFs displayed a higher GSVA score indicating their enhanced recapitulation of the specific activated fibroblast transcriptome (Fig. 1H). The M-TCP-iCFs also displayed an elevated GSVA score for 2 fibroblast populations. Both fibroblast populations showed higher enrichment for general fibroblast phenotypes (e.g., "GO-1903053: regulation of extracellular matrix organization"), suggesting that M-TCP-iCFs have enhanced ECM-related functions (Fig. 1I). Additionally, "Pid Integrin5 Pathway" showed shared expression between activated fibroblasts and upregulated genes in M-TCP-iCFs suggesting that the M-TCP conditions may foster similar overexpression of integrins, known to influence the behavior of fibroblasts during pathogenesis [59]. In summary, M-TCP-iCFs displayed a higher transcriptomic similarity to activated cardiac fibroblasts and heterogenous populations of DCM fibroblasts than healthy-CFs.

3.2. HEM supports cardiac fibroblasts differentiation

The activated fibroblast phenotype of M-TCP-iCFs can be attributed to the pathogenic cell culture conditions during and after the differentiation of hiPSC-CFs. To limit the activation of hiPSC-CFs, we hypothesized that a biomimetic substrate composed of cardiac-specific matrisomal proteins would provide a more biomimetic ECM environment during differentiation and expansion. We utilized porcine heart

extracellular matrix (HEM) as an alternative to Matrigel and uncoated TCP during and after differentiation, respectively. HEM has demonstrated efficacy in enhancing induced cardiomyocyte differentiation from cardiac fibroblasts in a 3D environment [39]. Compared to HEM, we found that Matrigel contains matrisome-associated protein SPARC (Fig. 2A). SPARC is a well-known inducer of activated fibroblasts and fibrosis [60–63]. SPARC plays a critical role in the activation of fibroblasts through crosstalk with TGFβ signaling [64] where a decrease in SPARC expression leads to decreased TGFβ expression [65]. and thus, less activation stimuli. Further, the crosstalk between fibronectin and SPARC has also been shown to activate fibroblasts [66]. As Matrigel contains both fibronectin and SPARC (Fig. 2A) and SPARC's role in TGFβ signaling, Matrigel may induce activation of cardiac fibroblasts through SPARC.

During heart development, epicardial cells depolarize and dissociate from the basement membrane of epicardium then migrate into the underlying myocardium to differentiate into cardiac fibroblasts [67,68]. These newly formed cardiac fibroblasts are quiescent and gradually maintain healthy ECM surrounding the cardiomyocytes. Meanwhile, deriving hiPSC-CFs *in vitro* typically occurs on Matrigel and then expanded on TCP [26,54,69]. Thus, current methods of differentiating hiPSC-CFs may induce pathogenic activation. Further, one study utilized

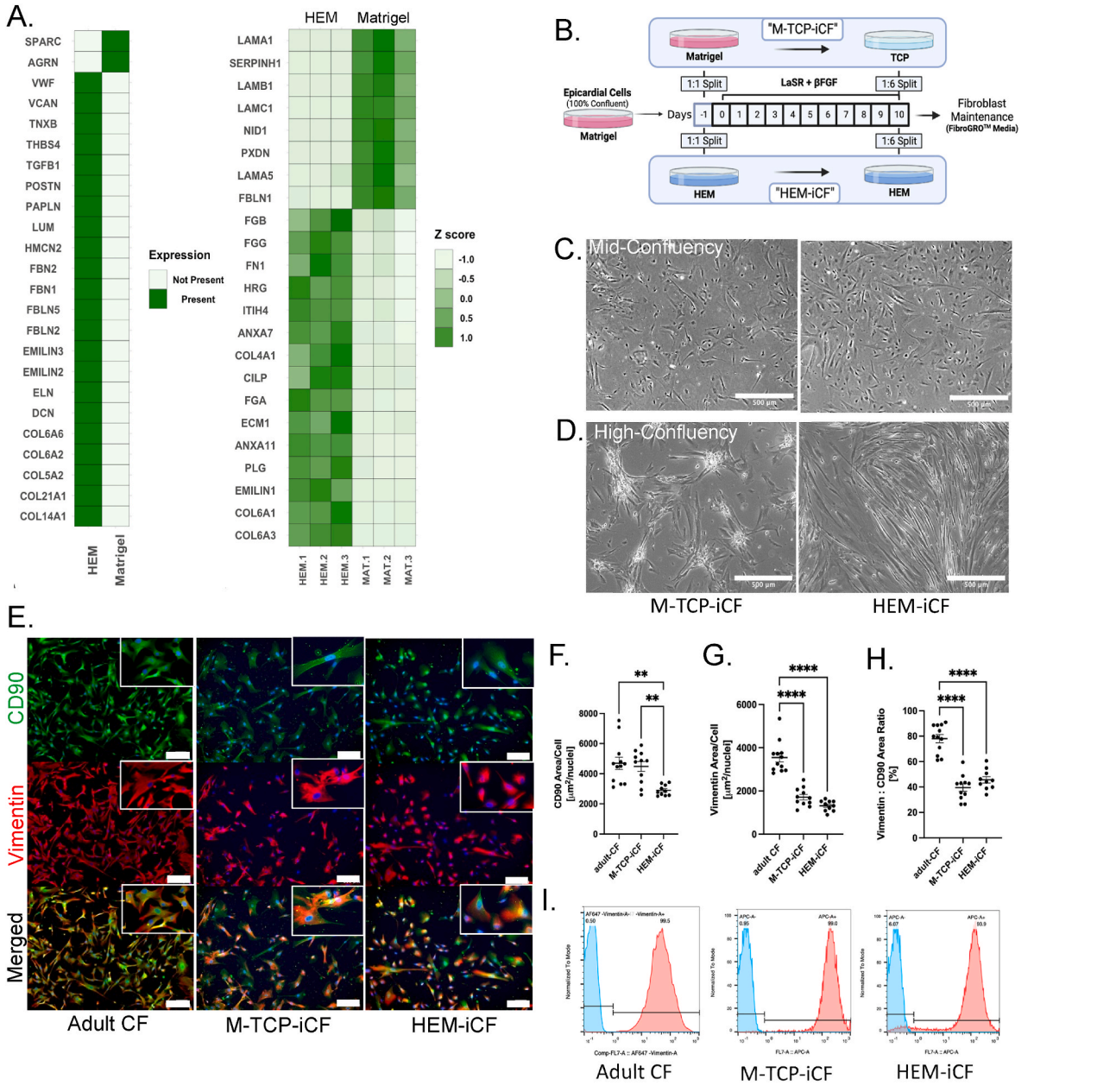

Fig. 2. HEM supports cardiac fibroblast differentiation

(A) Proteomic comparison of ECM proteins uniquely expressed (left) and differentially expressed (right) in Matrigel (n = 3) and HEM (n = 3). Differential expressed proteins exhibited a |log2fold| > 1.33 and a p-value <0.05. Adapted from [39]. (B) Schematic of the hiPSC-CF differentiation protocol on Matrigel or HEM. From D0 to D10, cells were treated with 10 ng/mL of βFGF in LaSR. Brightfield images of hiPSC-CF at (C) mid-confluency and (D) high confluency. Scale bars indicate 500 μm. (E) Immunofluorescent images of adult CF and hiPSC-CF of vimentin (red) and CD90 (green). Scale bar indicate 200 μM. Inlets depict higher magnification. (F) Measured CD90 expression, (G) Vimentin expression per cell per field of view and (H) Ratio of Vimentin to CD90 per field of view of adult-CF (n = 12), M-TCP-iCF (n = 11), and HEM-iCF (n = 10). ANOVA statistical analysis with Tukey's multiple comparison. ****p < 0.0001; **p < 0.01. (I) Floy cytometry analysis of vimentin expression.

TGFβ inhibition during and after differentiation to generate less activated cardiac fibroblasts [54], implying the inherent activation stimuli of Matrigel and TCP. To develop a more biomimetic strategy for hiPSC-CF derivation, we differentiated hiPSC-CFs on HEM and passaged them on HEM coated TCP (HEM-iCF), (Fig. 2B). To evaluate the effects of the HEM substrates on HEM-iCFs, we first assessed broad changes in cell morphology and expression of the known cardiac fibroblast markers, Vimentin and CD90 [6]. At low confluency, there appeared to be minor morphological differences between M-TCP-iCFs and HEM-iCFs (Fig. 2C). Yet, M-TCP-iCFs formed cell clusters at high confluency suggesting that HEM promotes enhanced cell attachment (Fig. 2D). HEM-iCFs also displayed a reduction in cell size but an improvement in size homogeneity, utilizing CD90 expression as a cell membrane marker (Fig. 2E and F). Interestingly, stiffer substrates have been shown to increase cell size [70] and mechanically stimulate the activation of cardiac fibroblasts [70–72]. Thus, HEM may reduce mechanical stress on the HEM-iCFs during expansion on TCP. Vimentin expression per cell and per cell size was not significantly different (Fig. 2G and 2H), suggesting no adverse changes to cardiac fibroblast phenotypes on HEM. Flow cytometry of vimentin confirmed HEM does not affect purity of hiPSC-CFs (Fig. 2I). Thus, while HEM reduces the cell size of hiPSC-CFs, it does not appear to adversely impair hiPSC-CF differentiation. Further, a larger cell size is not only associated with stiffer substrates, but also a characteristic of activated fibroblasts [73]. Thus, we hypothesized that the homeostatic ECM components found in HEM do not stimulate fibroblast activation when compared to SPARC-containing Matrigel and uncoated TCP.

3.3. HEM alleviates cardiac fibroblast activation during differentiation and expansion

To investigate if HEM can restrict hiPSC-CF activation, we examined expression of known activated cardiac fibroblast markers on the last day of differentiation (Day 10). We measured gene expression of *ACTA2*, *COL1A1* and *TGFB1*, all hallmark genes reported to be upregulated in activated fibroblasts [73]. Compared to Matrigel, hiPSC-CFs differentiated on HEM displayed reduced expression of the hallmark activated fibroblast genes (Fig. 3A), indicating HEM can restrict activation during hiPSC-CF differentiation. HEM-iCFs also had reduced expression of the activation hallmark genes compared to M-TCP-iCFs when passaged onto fresh cell culture substrates (Fig. 3B), indicating HEM can maintain the reduction in activation versus non-coated TCP. Additionally, HEM reduced the activation of hiPSC-CFs differentiated on Matrigel (M-HEM-iCFs) suggesting that HEM can relieve the activation already induced through cell culture conditions. This was further confirmed by replating low and higher passage M-TCP-iCFs onto HEM, which resulted in a reduction in *ACTA2*, *COL1A1*, *TGFB1* (Supplementary Fig. 2). Meanwhile, HEM-iCFs exhibited the most robust reduction in activated fibroblast gene expression in comparison to M-HEM-iCFs. In support of our gene expression assays, protein expression analysis for α-smooth muscle actin (αSMA), encoded by *ACTA2*, revealed lower expression in HEM-iCFs than M-TCP-iCFs (Fig. 3C and D), supporting the lack of an activated fibroblast phenotype in HEM-iCFs. As αSMA is a contractile cytoskeletal protein, we performed a collagen contraction assay to assess the functional properties of hiPSC-CFs. While not significant, collagen gels embedded with HEM-iCFs did show a slightly larger collagen area compared to M-TCP-iCFs (Fig. 3E and F). As the HEM-iCFs expressed minimal levels of αSMA, we speculate that the HEM-iCFs retain some contractile function, though lower than M-TCP-iCFs. Further, this suggests that HEM-iCF can maintain their inactivation in 3D environments, which is important for downstream applications in engineered cardiac microtissues. To further assess if HEM-iCFs can maintain reduced activation in the presence of activation stimuli, HEM-iCFs were passaged onto uncoated TCP. HEM-iCFs plated onto TCP had reduced *ACTA2* expression compared to M-TCP-iCFs (Fig. 3G). To further assess their phenotype in 3D self-assembling microtissue models, hiPSC-CF spheroids were fabricated with M-TCP-iCFs and HEM-iCFs. HEM-iCFs formed less aggregated spheroids (Fig. 3H and I) and reduced *ACTA2* expression in comparison to M-TCP-iCFs (Fig. 3J). Taken together, this suggests HEM-iCFs maintain less activated phenotype when implemented into 3D culture environments. In summary, HEM reduced the expression of activation markers during differentiation and passaging of hiPSC-CF which can be maintained both in the presence of activating stimuli and in 3D constructs. Thus, HEM enhances hiPSC-CF differentiation compared to standard practices on Matrigel and uncoated TCPs.

3.4. HEM-iCF have enhanced biomimicry in isogenic cardiac model

For disease modeling, many engineered cardiac tissues depend on the successful integration of several cell types found in the heart to successfully recapitulate native myocardium [32,74]. To assess the ability of HEM-iCFs for applications in engineered cardiac microtissues, we integrated HEM-iCFs into a 3D, isogenic cardiac organoid model. Briefly, hiPSC-CMs, hiPSC-CFs and hiPSC-ECs were mixed at a ratio of 70:15:15 (hiPSC-CM: hiPSC-CF: hiPSC-EC) to fabricate cardiac organoids based on our previously established cardiac microtissue fabrication method [31,51,52]. In comparison to M-TCP-iCFs, HEM-iCFs demonstrated more homogenous integration into the cardiac organoids (Fig. 4A). While there was no total change in Vimentin expression (Fig. 4C), the HEM-iCFs had a significantly improved homogeneity within the organoids, particularly enhanced in the core regions (Fig. 4B). This suggests an enhanced recapitulation of cardiac fibroblast and cardiomyocyte interactions in myocardium, in which cardiomyocytes and cardiac fibroblasts are homogenously distributed [75]. As activated fibroblast can impair cardiomyocyte function via physical contact and paracrine factors, like TGFβ [75], we investigated the impacts of HEM-iCFs versus M-TCP-iCFs on hiPSC-CMs within the organoid model. HEM-iCFs were shown to enhance expression of α−sarcomeric actinin (αSA), a cardiac-specific contractile protein and biomarker, through the whole organoid in comparison to M-TCP-iCFs (Fig. 4A and D). This increase in αSA expression suggests that HEM-iCFs might improve hiPSC-CM contractile development within the isogenic model. However, while αSA expression increased in the HEM-iCFs organoids, organoid contractility, defined as the fractional area change (FAC) was reduced (Fig. 4E). The divergence between increased αSA expression and contractility might be influenced by the location of hiPSC-CFs with the organoid. For example, more internally located HEM-iCFs could increase the internal stiffness of the cardiac organoids compared to peripherally organized M-TCP-iCFs. Thus, a higher internal stiffness may reduce the compliance of the organoids and manifest as a reduction in FAC. Previous reports show that activated fibroblasts also exhibit angiogenic properties involved in several pathologies [76]. In agreement with this, cardiac organoids with HEM-iCFs showed a reduction in CD31 expression, a marker of hiPSC-ECs, compared to those with M-TCP-iCFs (Fig. 4F and G). Thus, further highlighting that HEM-iCFs phenotype is more aligned with a steady state fibroblast versus the activated phenotype represented by M-TCP-iCFs. In summary, HEM-iCFs can promote cardiomyocyte development and a nonpathogenic cardiac microtissue.

4. Conclusion

Here, we demonstrate that HEM-coated TCP enhances hiPSC-CF differentiation and expansion. M-TCP-iCFs are more transcriptomically similar with DCM-CFs than healthy-CF, and exhibit an elevated enrichment for activated fibroblast gene expression pathways. Activation of hiPSC-CFs may be due, at least in part, to the presence of SPARC within Matrigel followed by expansion on TCP, a mechanical inducer of fibroblast activation. We show that HEM inhibits the activation of hiPSC-CF during differentiation and maintained the reduction in activation during expansion. In support of this, HEM-iCFs show reductions in αSMA expression, a functional marker of an activated fibroblast.

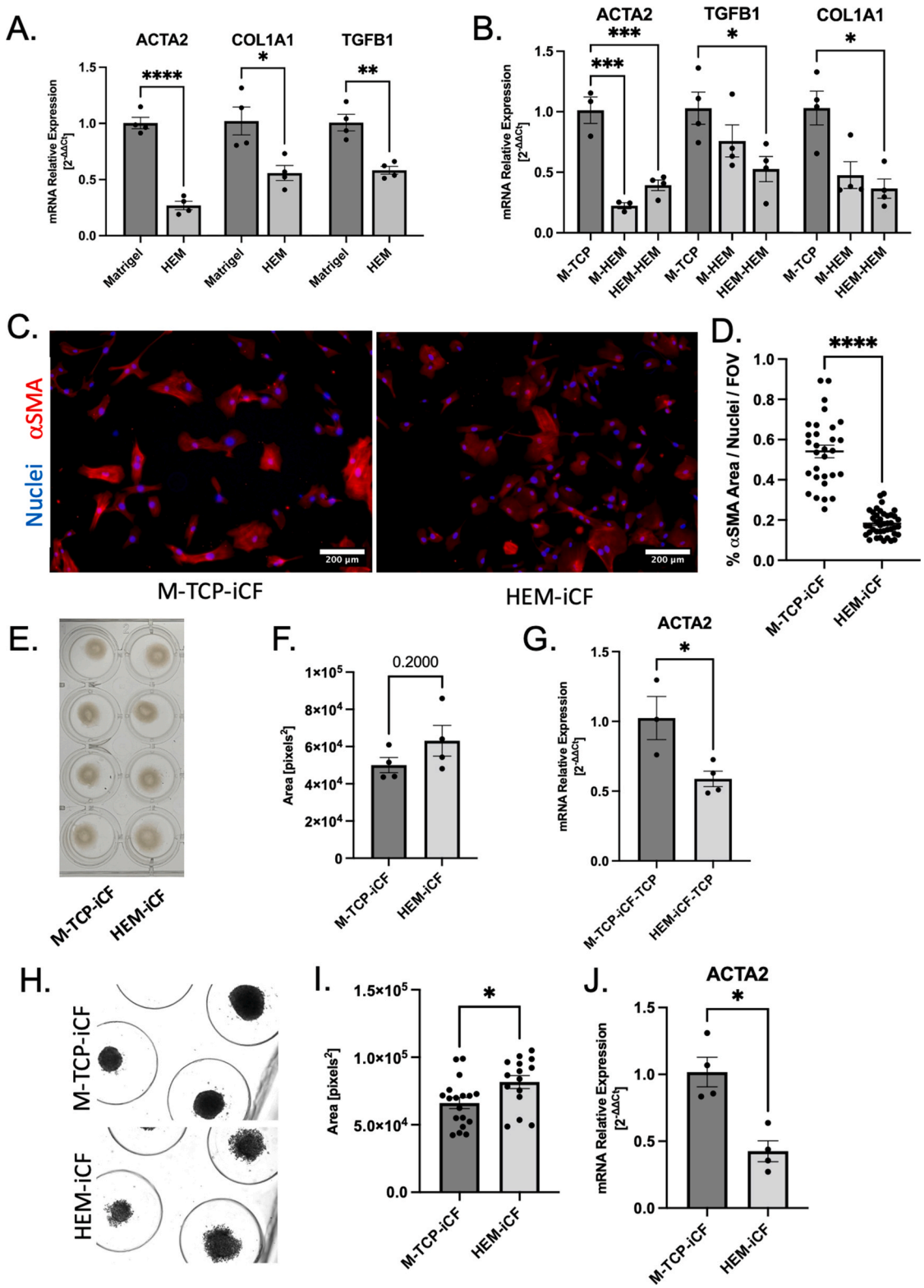

Fig. 3. HEM prevents and alleviates the activation of hiPSC-CF

(A) RT-qPCR of hallmark activated fibroblast genes of hiPSC-CF on D10 of differentiation. Students t-test. (B) RT-qPCR of activated fibroblast genes of hiPSC-CF passaged onto TCP or HEM after D10 of differentiation. M-HEM denotes hiPSC-CF differentiated on Matrigel then passaged onto HEM. One-way ANOVA with Tukey's multiple comparison test. (C) αSMA protein (red) expression of hiPSC-CF. Scale bar indicates 200 μm. (D) Quantification of αSMA expression per nuclei per field of view (FOV). Student's t-test. (E) Representative image of collagen contraction assay of hiPSC-CF in 24-well plate. (F) Collagen area of collagen contraction assay. (G) RT-qPCR of hiPSC-CF seeded onto uncoated TCP. Student's t-test. (H) Spheroids fabricated using hiPSC-CF. (I) Quantification of area of hiPSC-CF spheroids. Student's t-test. (J) RT-qPCR of hiPSC-CF spheroids. ****$p < 0.0001$; ***$p < 0.001$; **$p < 0.01$; *$p < 0.05$.

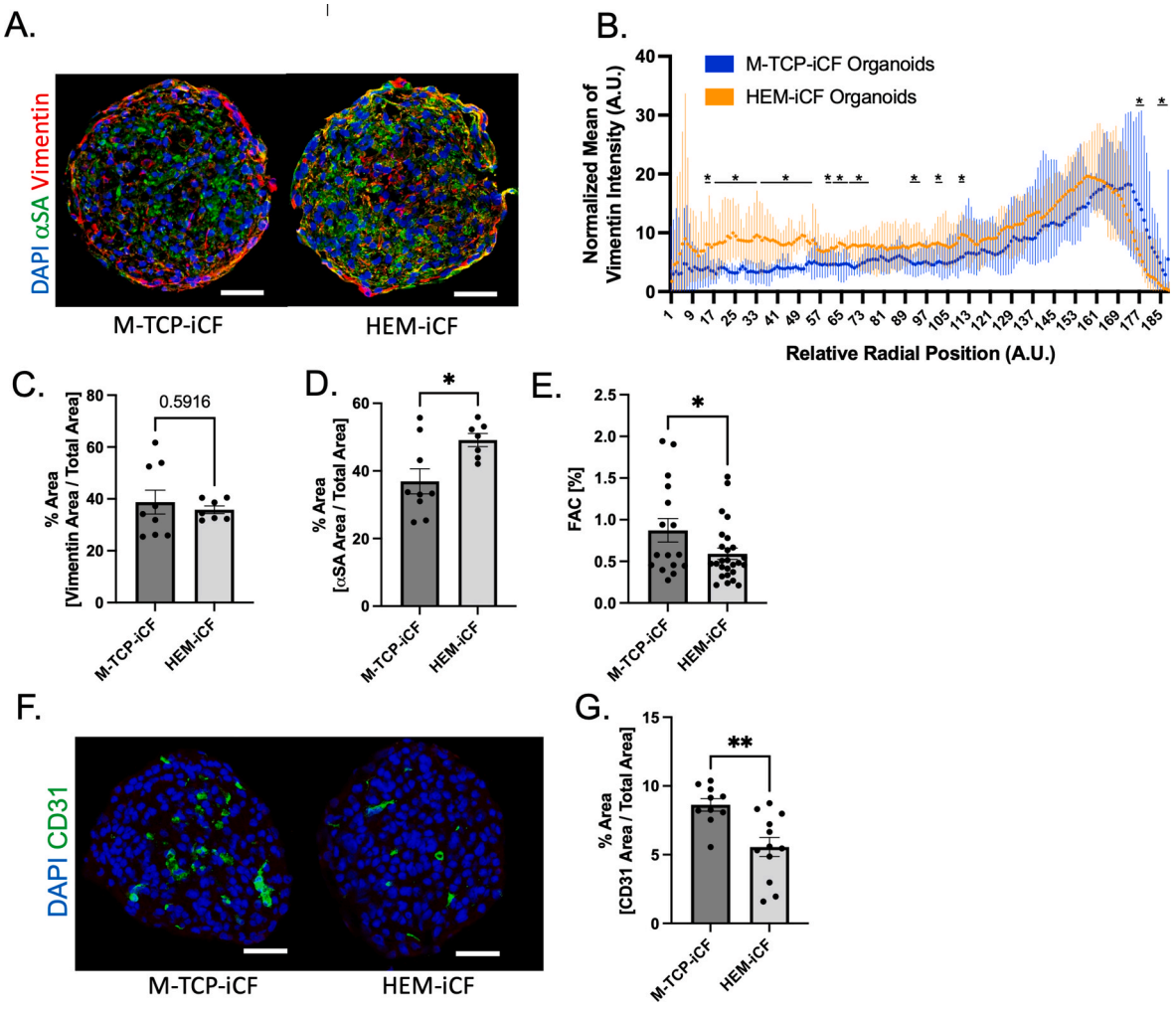

Fig. 4. HEM-iCF have improved biomimicry in hiPSC-cardiac organoid model.
(A) Representative images of hiPSC-cardiac organoids composed of 70% hiPSC-CMs, 15% hiPSC-ECs and 15% of either M-TCP-iCFs or HEM-iCFs. Organoids were embedded 14 days after fabrication and stained for hiPSC-CM using α-sarcomeric actinin (αSA) (green), hiPSC-CFs using Vimentin (red) and nuclei (blue). Scale bar indicates 100 μm. (B) Radial intensity of vimentin expression across organoids. Student's t-test. (C) Percent area of vimentin expression and (D) αSA expression normalized to the area of the organoids. Student's t-test. (E) Fractional Area Change (FAC) of contracting hiPSC-cardiac organoids. (F) Representative images of hiPSC-cardiac organoids stained for hiPSC-EC using CD31 (green) and nuclei (blue). Scale bar indicates 100 μm. (G) Percent area of CD31 expression normalized to area of the organoids. Student's t-test (M-TCP-iCF: n = 11; HEM-iCF: n = 12).

Further, HEM alleviated the activation of M-TCP-iCFs. Lastly, isogenic cardiac organoids fabricated with HEM-iCFs recapitulated homogenous cardiomyocyte and cardiac fibroblast interactions, improved the contractile development of cardiomyocytes, and demonstrated a reduction in angiogenesis, a hallmark of activated fibroblasts. In summary, we show that the hiPSC-iCF phenotype supported by HEM is more consistent with a homeostatic fibroblast phenotype than hiPSC-CFs differentiated on Matrigel and expanded on TCP. As recent investigations have shown that HEM can improve cardiomyocyte phenotypes during direct differentiation techniques [39], future investigations into the impact of HEM on additional cardiac cell types may also reveal enhanced differentiation capabilities given the biomimetic nature of HEM. Further, coupling HEM to transplantable materials, such as aerogels, may provide enhanced pro-reparative constructs for treating cardiovascular disease. Thus, HEM-iCFs have great potential to aid in the development higher fidelity hiPSC cardiac tissue constructs for cardiotoxicity screening and disease modeling applications.

Ethics approval and consent to participate

Not applicable.

Author contributions

Charles M. Kerr: Conceptualization, Data curation, Formal analysis, Funding acquisition, Investigation, Methodology, Project administration, Resources, Software, Supervision, Visualization, Roles/Writing - original draft, Writing - review & editing.

Sophia E. Silver: Formal analysis, Investigation, Methodology, Data curation, Writing - review & editing.

Martha Floy: Conceptualization, Methodology, Resources.

Yi Sun Choi: Formal analysis, Data curation, Investigation, Resources, Software.

Amy E. Bradshaw: Resources, Supervision.

Sean Palecek: Conceptualization, Methodology, Resources, Funding acquisition.

Seung-Woo Cho: Methodology, Resources, Funding acquisition.

Ying Mei: Conceptualization, Funding acquisition; Project administration; Resources, Supervision, Roles/Writing - original draft, Writing - review & editing.

Declaration of competing interest

The authors declare that they have no known competing financial interests or personal relationships that could have appeared to influence the work reported in this paper.

Acknowledgements

We sincerely thank the previous and current members of Dr. Sean Palecek's laboratory at the University of Wisconsin-Madison and Drs. Sharon Gerecht and Rahel Schnellmann at Duke University, for their assistance in hiPSC-cardiac cell differentiations and stem cell culture techniques. This research was funded by the National Institutes of Health (NIH) F31 HL154665, R01 HL133308, 8P20 GM103444, R21 HL167211, R01 HL168255, U01 HL169361, R01 HL148059, the NIH Cardiovascular Training Grant T32 HL007260, the National Science Foundation (NSF) (CBET-1743346), the NSF Engineering Research Center for Cell Manufacturing Technologies (CMaT; NSF EEC-1648035) and the VA Merit I01 BX005943-01A1. This research was also supported by the grants, 2021R1A2C3004262. and 2022M3A9B6082675, of the National Research Foundation of Korea (NRF) funded by the Korean government, the Ministry of Science and ICT (MSIT). This study used the services of the Morphology, Imaging and Instrumentation Core, which is supported by NIH-NIGMS P30 GM103342 to the South Carolina COBRE for Developmentally Based Cardiovascular Diseases.

Appendix A. Supplementary data

Supplementary data to this article can be found online at https://doi.org/10.1016/j.bioactmat.2023.08.023.

References

[1] M Vaduganathan, A Mensah George, V Turco Justine, V Fuster, Gregory A Roth, The Global Burden of Cardiovascular Diseases and Risk, J. Am. Coll. Cardiol. 80 (2022) 2361–2371.
[2] O.A. Centurión, J.F. Alderete, J.M. Torales, L.B. García, K.E. Scavenius, L.M. Miño, Myocardial fibrosis as a pathway of prediction of ventricular arrhythmias and sudden cardiac death in patients with nonischemic dilated cardiomyopathy, Crit. Pathw. Cardiol. 18 (2) (2019) 89–97, https://doi.org/10.1097/hpc.0000000000000171.
[3] R. Dweck Marc, S. Joshi, T. Murigu, F. Alpendurada, A. Jabbour, G. Melina, K. Prasad Sanjay, Midwall fibrosis is an independent predictor of mortality in patients with aortic stenosis, J. Am. Coll. Cardiol. 58 (12) (2011) 1271–1279, https://doi.org/10.1016/j.jacc.2011.03.064.
[4] A. Zegard, O. Okafor, J. de Bono, M. Kalla, M. Lencioni, H. Marshall, F. Leyva, Myocardial fibrosis as a predictor of sudden death in patients with coronary artery disease, J. Am. Coll. Cardiol. 77 (1) (2021) 29–41, https://doi.org/10.1016/j.jacc.2020.10.046.
[5] M. Lockhart, E. Wirrig, A. Phelps, A. Wessels, Extracellular matrix and heart development, Birth Defects Res A Clin Mol Teratol 91 (6) (2011) 535–550, https://doi.org/10.1002/bdra.20810.
[6] V. Talman, H. Ruskoaho, Cardiac fibrosis in myocardial infarction-from repair and remodeling to regeneration, Cell Tissue Res. 365 (3) (2016) 563–581, https://doi.org/10.1007/s00441-016-2431-9.
[7] J.G. Travers, F.A. Kamal, J. Robbins, K.E. Yutzey, B.C. Blaxall, Cardiac fibrosis: the fibroblast awakens, Circ. Res. 118 (6) (2016) 1021–1040, https://doi.org/10.1161/CIRCRESAHA.115.306565.
[8] S. Maruyama, K. Nakamura, K.N. Papanicolaou, S. Sano, I. Shimizu, Y. Asaumi, K. Walsh, Follistatin-like 1 promotes cardiac fibroblast activation and protects the heart from rupture, EMBO Mol. Med. 8 (8) (2016) 949–966, https://doi.org/10.15252/emmm.201506151.
[9] A.R. Perestrelo, A.C. Silva, J. Oliver-De La Cruz, F. Martino, V. Horvath, G. Caluori, G. Forte, Multiscale analysis of extracellular matrix remodeling in the failing heart, Circ. Res. 128 (1) (2021) 24–38, https://doi.org/10.1161/CIRCRESAHA.120.317685.
[10] K. Blinova, D. Schocken, D. Patel, C. Daluwatte, J. Vicente, J.C. Wu, D.G. Strauss, Clinical trial in a dish: personalized stem cell–derived cardiomyocyte assay compared with clinical trial results for two QT-prolonging drugs, Clinical and Translational Science 12 (6) (2019) 687–697, https://doi.org/10.1111/cts.12674.
[11] K.O. Brandão, L. van den Brink, D.C. Miller, C. Grandela, B.J. van Meer, M.P. H. Mol, R.P. Davis, Isogenic sets of hiPSC-CMs harboring distinct KCNH2 mutations differ functionally and in susceptibility to drug-induced arrhythmias, Stem Cell Rep. 15 (5) (2020) 1127–1139, https://doi.org/10.1016/j.stemcr.2020.10.005.
[12] P.W. Burridge, Y.F. Li, E. Matsa, H. Wu, S.G. Ong, A. Sharma, J.C. Wu, Human induced pluripotent stem cell-derived cardiomyocytes recapitulate the predilection of breast cancer patients to doxorubicin-induced cardiotoxicity, Nat. Med. 22 (5) (2016) 547–556, https://doi.org/10.1038/nm.4087.
[13] N. Sun, M. Yazawa, J. Liu, L. Han, V. Sanchez-Freire, O.J. Abilez, J.C. Wu, Patient-specific induced pluripotent stem cells as a model for familial dilated cardiomyopathy, Sci. Transl. Med. 4 (130) (2012), 130ra147, https://doi.org/10.1126/scitranslmed.3003552.
[14] C.R. Archer, R. Sargeant, J. Basak, J. Pilling, J.R. Barnes, A. Pointon, Characterization and validation of a human 3D cardiac microtissue for the assessment of changes in cardiac pathology, Sci. Rep. 8 (1) (2018), 10160, https://doi.org/10.1038/s41598-018-28393-y.
[15] T.J. Owen, S.E. Harding, Multi-cellularity in cardiac tissue engineering, how close are we to native heart tissue? J. Muscle Res. Cell Motil. 40 (2) (2019) 151–157, https://doi.org/10.1007/s10974-019-09528-8.
[16] L. Polonchuk, M. Chabria, L. Badi, J.C. Hoflack, G. Figtree, M.J. Davies, C. Gentile, Cardiac spheroids as promising in vitro models to study the human heart microenvironment, Sci. Rep. 7 (1) (2017) 7005, https://doi.org/10.1038/s41598-017-06385-8.
[17] H.K. Kleinman, G.R. Martin, Matrigel: basement membrane matrix with biological activity, Semin. Cancer Biol. 15 (5) (2005) 378–386, https://doi.org/10.1016/j.semcancer.2005.05.004.
[18] J.-J. Santiago, A.L. Dangerfield, S.G. Rattan, K.L. Bathe, R.H. Cunnington, J. E. Raizman, I.M.C. Dixon, Cardiac fibroblast to myofibroblast differentiation in vivo and in vitro: expression of focal adhesion components in neonatal and adult rat ventricular myofibroblasts, Dev. Dynam. 239 (6) (2010) 1573–1584, https://doi.org/10.1002/dvdy.22280.
[19] D. Bejleri, M.E. Davis, Decellularized extracellular matrix materials for cardiac repair and regeneration, Adv. Healthcare Mater. 8 (5) (2019), e1801217, https://doi.org/10.1002/adhm.201801217.
[20] D. Bejleri, B.W. Streeter, A.L.Y. Nachlas, M.E. Brown, R. Gaetani, K.L. Christman, M.E. Davis, A bioprinted cardiac patch composed of cardiac-specific extracellular matrix and progenitor cells for heart repair, Adv. Healthcare Mater. 7 (23) (2018), e1800672, https://doi.org/10.1002/adhm.201800672.
[21] T.J. Keane, I.T. Swinehart, S.F. Badylak, Methods of tissue decellularization used for preparation of biologic scaffolds and in vivo relevance, Methods 84 (2015) 25–34, https://doi.org/10.1016/j.ymeth.2015.03.005.
[22] F.G. Scholl, M.M. Boucek, K.C. Chan, L. Valdes-Cruz, R. Perryman, Preliminary experience with cardiac reconstruction using decellularized porcine extracellular matrix scaffold: human applications in congenital heart disease, World J Pediatr Congenit Heart Surg 1 (1) (2010) 132–136, https://doi.org/10.1177/2150135110362092.
[23] G. Agmon, K.L. Christman, Controlling stem cell behavior with decellularized extracellular matrix scaffolds, Curr. Opin. Solid State Mater. Sci. 20 (4) (2016) 193–201, https://doi.org/10.1016/j.cossms.2016.02.001.
[24] S. Higuchi, Q. Lin, J. Wang, T.K. Lim, S.B. Joshi, G.S. Anand, H. Fujita, Heart extracellular matrix supports cardiomyocyte differentiation of mouse embryonic stem cells, J. Biosci. Bioeng. 115 (3) (2013) 320–325, https://doi.org/10.1016/j.jbiosc.2012.10.004.
[25] E.L. Krug, C.H. Mjaatvedt, R.R. Markwald, Extracellular matrix from embryonic myocardium elicits an early morphogenetic event in cardiac endothelial differentiation, Dev. Biol. 120 (2) (1987) 348–355, https://doi.org/10.1016/0012-1606(87)90237-5.
[26] M.E. Floy, S.E. Givens, O.B. Matthys, T.D. Mateyka, C.M. Kerr, A.B. Steinberg, S. P. Palecek, Developmental lineage of human pluripotent stem cell-derived cardiac fibroblasts affects their functional phenotype, FASEB J. 35 (9) (2021), e21799, https://doi.org/10.1096/fj.202100523R.
[27] X. Bao, X. Lian, T.A. Hacker, E.G. Schmuck, T. Qian, V.J. Bhute, S.P. Palecek, Long-term self-renewing human epicardial cells generated from pluripotent stem cells under defined xeno-free conditions, Nat. Biomed. Eng. 1 (2016), https://doi.org/10.1038/s41551-016-0003.
[28] Y. Zhang, G. Parmigiani, W.E. Johnson, ComBat-seq: batch effect adjustment for RNA-seq count data, NAR Genom Bioinform 2 (3) (2020), lqaa078, https://doi.org/10.1093/nargab/lqaa078.
[29] R.C. Gentleman, V.J. Carey, D.M. Bates, B. Bolstad, M. Dettling, S. Dudoit, J. Zhang, Bioconductor: open software development for computational biology and bioinformatics, Genome Biol. 5 (10) (2004) R80, https://doi.org/10.1186/gb-2004-5-10-r80.
[30] W. Huber, V.J. Carey, R. Gentleman, S. Anders, M. Carlson, B.S. Carvalho, M. Morgan, Orchestrating high-throughput genomic analysis with Bioconductor, Nat. Methods 12 (2) (2015) 115–121, https://doi.org/10.1038/nmeth.3252.
[31] D.J. Richards, Y. Li, C.M. Kerr, J. Yao, G.C. Beeson, R.C. Coyle, Y. Mei, Human cardiac organoids for the modelling of myocardial infarction and drug cardiotoxicity, Nat. Biomed. Eng. 4 (4) (2020) 446–462, https://doi.org/10.1038/s41551-020-0539-4.
[32] C.M. Kerr, D. Richards, D.R. Menick, K.Y. Deleon-Pennell, Y. Mei, Multicellular Human Cardiac Organoids Transcriptomically Model Distinct Tissue-Level Features of Adult Myocardium, Int. J. Mol. Sci. 22 (16) (2021), https://doi.org/10.3390/ijms22168482.
[33] M.I. Love, W. Huber, S. Anders, Moderated estimation of fold change and dispersion for RNA-seq data with DESeq2, Genome Biol. 15 (12) (2014) 550, https://doi.org/10.1186/s13059-014-0550-8.
[34] C. Ginestet, ggplot2: elegant graphics for data analysis, J. Roy. Stat. Soc. 174 (1) (2011) 245–246, https://doi.org/10.1111/j.1467-985X.2010.00676_9.x.
[35] V.K. Mootha, C.M. Lindgren, K.F. Eriksson, A. Subramanian, S. Sihag, J. Lehar, L. C. Groop, PGC-1alpha-responsive genes involved in oxidative phosphorylation are coordinately downregulated in human diabetes, Nat. Genet. 34 (3) (2003) 267–273, https://doi.org/10.1038/ng1180.

[36] A. Subramanian, P. Tamayo, V.K. Mootha, S. Mukherjee, B.L. Ebert, M.A. Gillette, J.P. Mesirov, Gene set enrichment analysis: a knowledge-based approach for interpreting genome-wide expression profiles, Proc. Natl. Acad. Sci. U.S.A. 102 (43) (2005) 15545–15550, https://doi.org/10.1073/pnas.0506580102.
[37] Y. Zhou, B. Zhou, L. Pache, M. Chang, A.H. Khodabakhshi, O. Tanaseichuk, S. K. Chanda, Metascape provides a biologist-oriented resource for the analysis of systems-level datasets, Nat. Commun. 10 (1) (2019) 1523, https://doi.org/10.1038/s41467-019-09234-6.
[38] M. Chaffin, I. Papangeli, B. Simonson, A.D. Akkad, M.C. Hill, A. Arduini, P. T. Ellinor, Single-nucleus profiling of human dilated and hypertrophic cardiomyopathy, Nature (2022), https://doi.org/10.1038/s41586-022-04817-8.
[39] Y. Jin, H. Kim, S. Min, Y.S. Choi, S.J. Seo, E. Jeong, S.W. Cho, Three-dimensional heart extracellular matrix enhances chemically induced direct cardiac reprogramming, Sci. Adv. 8 (50) (2022), eabn5768, https://doi.org/10.1126/sciadv.abn5768.
[40] X. Lian, J. Zhang, S.M. Azarin, K. Zhu, L.B. Hazeltine, X. Bao, S.P. Palecek, Directed cardiomyocyte differentiation from human pluripotent stem cells by modulating Wnt/beta-catenin signaling under fully defined conditions, Nat. Protoc. 8 (1) (2013) 162–175, https://doi.org/10.1038/nprot.2012.150.
[41] X. Bao, X. Lian, T. Qian, V.J. Bhute, T. Han, S.P. Palecek, Directed differentiation and long-term maintenance of epicardial cells derived from human pluripotent stem cells under fully defined conditions, Nat. Protoc. 12 (9) (2017) 1890–1900, https://doi.org/10.1038/nprot.2017.080.
[42] D.J. Richards, Y. Tan, R. Coyle, Y. Li, R. Xu, N. Yeung, Y. Mei, Nanowires and Electrical Stimulation Synergistically Improve Functions of hiPSC Cardiac Spheroids, Nano. Lett. 16 (7) (2016) 4670–4678, https://doi.org/10.1021/acs.nanolett.6b02093.
[43] Y. Tan, D. Richards, R.C. Coyle, J. Yao, R. Xu, W. Gou, Y. Mei, Cell number per spheroid and electrical conductivity of nanowires influence the function of silicon nanowired human cardiac spheroids, Acta Biomater. 51 (2017) 495–504, https://doi.org/10.1016/j.actbio.2017.01.029.
[44] Y. Tan, D. Richards, R. Xu, S. Stewart-Clark, S.K. Mani, T.K. Borg, Y. Mei, Silicon nanowire-induced maturation of cardiomyocytes derived from human induced pluripotent stem cells, Nano. Lett. 15 (5) (2015) 2765–2772, https://doi.org/10.1021/nl502227a.
[45] S. Tohyama, F. Hattori, M. Sano, T. Hishiki, Y. Nagahata, T. Matsuura, K. Fukuda, Distinct metabolic flow enables large-scale purification of mouse and human pluripotent stem cell-derived cardiomyocytes, Cell Stem Cell 12 (1) (2013) 127–137, https://doi.org/10.1016/j.stem.2012.09.013.
[46] R.G.C. Maas, S. Lee, M. Harakalova, C.J.B. Snijders Blok, W.R. Goodyer, J. Hjortnaes, J.W. Buikema, Massive expansion and cryopreservation of functional human induced pluripotent stem cell-derived cardiomyocytes, STAR Protoc 2 (1) (2021), 100334, https://doi.org/10.1016/j.xpro.2021.100334.
[47] J.W. Buikema, S. Lee, W.R. Goodyer, R.G. Maas, O. Chirikian, G. Li, S.M. Wu, Wnt activation and reduced cell-cell contact synergistically induce massive expansion of functional human iPSC-derived cardiomyocytes, Cell Stem Cell 27 (1) (2020) 50–63 e55, https://doi.org/10.1016/j.stem.2020.06.001.
[48] H. Cho, B.L. Macklin, Y.Y. Lin, L. Zhou, M.J. Lai, G. Lee, E.J. Duh, iPSC-derived endothelial cell response to hypoxia via SDF1a/CXCR4 axis facilitates incorporation to revascularize ischemic retina, JCI Insight 5 (6) (2020), https://doi.org/10.1172/jci.insight.131828.
[49] Q. Smith, B. Macklin, X.Y. Chan, H. Jones, M. Trempel, M.C. Yoder, S. Gerecht, Differential HDAC6 activity modulates ciliogenesis and subsequent mechanosensing of endothelial cells derived from pluripotent stem cells, Cell Rep. 24 (4) (2018) 895–908 e896, https://doi.org/10.1016/j.celrep.2018.06.083.
[50] X. Bao, X. Lian, S.P. Palecek, Directed Endothelial Progenitor Differentiation from Human Pluripotent Stem Cells Via Wnt Activation Under Defined Conditions, Methods Mol. Biol. 1481 (2016) 183–196, https://doi.org/10.1007/978-1-4939-6393-5_17.
[51] D.J. Richards, R.C. Coyle, Y. Tan, J. Jia, K. Wong, K. Toomer, Y. Mei, Inspiration from heart development: Biomimetic development of functional human cardiac organoids, Biomaterials 142 (2017) 112–123, https://doi.org/10.1016/j.biomaterials.2017.07.021.
[52] R.C. Coyle, R.W. Barrs, D.J. Richards, E.P. Ladd, D.R. Menick, Y. Mei, Targeting HIF-α for robust prevascularization of human cardiac organoids, J. Tissue Eng. Regen. Med. (2020), https://doi.org/10.1002/term.3165.
[53] D.C. Arhontoulis, C.M. Kerr, D. Richards, K. Tjen, N. Hyams, J.A. Jones, Y. Mei, Human cardiac organoids to model COVID-19 cytokine storm induced cardiac injuries, J. Tissue. Eng. Regen Med. 16 (9) (2022) 799–811, https://doi.org/10.1002/term.3327.
[54] J. Zhang, R. Tao, K.F. Campbell, J.L. Carvalho, E.C. Ruiz, G.C. Kim, T.J. Kamp, Functional cardiac fibroblasts derived from human pluripotent stem cells via second heart field progenitors, Nat. Commun. 10 (1) (2019) 2238, https://doi.org/10.1038/s41467-019-09831-5.
[55] A.J. Whitehead, J.D. Hocker, B. Ren, A.J. Engler, Improved epicardial cardiac fibroblast generation from iPSCs, J. Mol Cell. Cardiol. 164 (2021) 58–68, https://doi.org/10.1016/j.yjmcc.2021.11.011.
[56] G.A. Roth, D. Abate, K.H. Abate, S.M. Abay, C. Abbafati, N. Abbasi, C.J.L. Murray, Global, regional, and national age-sex-specific mortality for 282 causes of death in 195 countries and territories, 1980–2017: a systematic analysis for the Global Burden of Disease Study 2017, Lancet 392 (10159) (2018) 1736–1788, https://doi.org/10.1016/s0140-6736(18)32203-7.
[57] M. Delcommenne, C.H. Streuli, Control of integrin expression by extracellular matrix, J. Biol. Chem. 270 (45) (1995) 26794–26801, https://doi.org/10.1074/jbc.270.45.26794.
[58] C.M. Benaud, R.B. Dickson, Regulation of the expression of c-Myc by beta1 integrins in epithelial cells, Oncogene 20 (6) (2001) 759–768, https://doi.org/10.1038/sj.onc.1204152.
[59] S.K. Agarwal, Integrins and cadherins as therapeutic targets in fibrosis, Front. Pharmacol. 5 (2014) 131.
[60] M. Bujak, N.G. Frangogiannis, The role of TGF-beta signaling in myocardial infarction and cardiac remodeling, Cardiovasc. Res. 74 (2) (2007) 184–195, https://doi.org/10.1016/j.cardiores.2006.10.002.
[61] H.H. Hu, D.Q. Chen, Y.N. Wang, Y.L. Feng, G. Cao, N.D. Vaziri, Y.Y. Zhao, New insights into TGF-beta/Smad signaling in tissue fibrosis, Chem. Biol. Interact. 292 (2018) 76–83, https://doi.org/10.1016/j.cbi.2018.07.008.
[62] H. Khalil, O. Kanisicak, V. Prasad, R.N. Correll, X. Fu, T. Schips, J.D. Molkentin, Fibroblast-specific TGF-beta-Smad2/3 signaling underlies cardiac fibrosis, J. Clin. Invest. 127 (10) (2017) 3770–3783, https://doi.org/10.1172/JCI94753.
[63] T. Liu, D. Song, J. Dong, P. Zhu, J. Liu, W. Liu, S. Ling, Current understanding of the pathophysiology of myocardial fibrosis and its quantitative assessment in heart failure, Front. Physiol. 8 (2017) 238, https://doi.org/10.3389/fphys.2017.00238.
[64] J. Trombetta-Esilva, A.D. Bradshaw, The function of SPARC as a mediator of fibrosis, Open Rheumatol. J. 6 (2012) 146–155, https://doi.org/10.2174/1874312901206010146.
[65] X. Zhou, F.K. Tan, X. Guo, D. Wallis, D.M. Milewicz, S. Xue, F.C. Arnett, Small interfering RNA inhibition of SPARC attenuates the profibrotic effect of transforming growth factor beta1 in cultured normal human fibroblasts, Arthritis Rheum. 52 (1) (2005) 257–261, https://doi.org/10.1002/art.20785.
[66] S. Yoshida, K. Asanoma, H. Yagi, I. Onoyama, E. Hori, Y. Matsumura, K. Kato, Fibronectin mediates activation of stromal fibroblasts by SPARC in endometrial cancer cells, BMC Cancer 21 (1) (2021) 156, https://doi.org/10.1186/s12885-021-07875-9.
[67] M.D. Tallquist, Cardiac fibroblasts: from origin to injury, Curr Opin Physiol 1 (2018) 75–79, https://doi.org/10.1016/j.cophys.2017.08.002.
[68] E.M. Zeisberg, R. Kalluri, Origins of cardiac fibroblasts, Circ. Res. 107 (11) (2010) 1304–1312, https://doi.org/10.1161/CIRCRESAHA.110.231910.
[69] H. Zhang, L. Tian, M. Shen, C. Tu, H. Wu, M. Gu, J.C. Wu, Generation of Quiescent Cardiac Fibroblasts From Human Induced Pluripotent Stem Cells for In Vitro Modeling of Cardiac Fibrosis, Circ Res. 125 (5) (2019) 552–566, https://doi.org/10.1161/CIRCRESAHA.119.315491.
[70] K.M. Herum, J. Choppe, A. Kumar, A.J. Engler, A.D. McCulloch, Mechanical regulation of cardiac fibroblast profibrotic phenotypes, Mol. Biol. Cell. 28 (14) (2017) 1871–1882, https://doi.org/10.1091/mbc.E17-01-0014.
[71] G. Gilles, A.D. McCulloch, C.H. Brakebusch, K.M. Herum, Maintaining resting cardiac fibroblasts in vitro by disrupting mechanotransduction, PLoS One 15 (10) (2020), e0241390, https://doi.org/10.1371/journal.pone.0241390.
[72] N.M. Landry, S.G. Rattan, I.M.C. Dixon, An improved method of maintaining primary murine cardiac fibroblasts in two-dimensional cell culture, Sci. Rep. 9 (1) (2019), 12889, https://doi.org/10.1038/s41598-019-49285-9.
[73] J. Baum, H.S. Duffy, Fibroblasts and myofibroblasts: what are we talking about? J. Cardiovasc. Pharmacol. 57 (4) (2011) 376–379, https://doi.org/10.1097/FJC.0b013e3182116e39.
[74] E. Giacomelli, V. Meraviglia, G. Campostrini, A. Cochrane, X. Cao, R.W.J. van Helden, C.L. Mummery, Human-iPSC-Derived cardiac stromal cells enhance maturation in 3D cardiac microtissues and reveal non-cardiomyocyte contributions to heart disease, Cell Stem Cell 26 (6) (2020) 862–879 e811, https://doi.org/10.1016/j.stem.2020.05.004.
[75] C. Hall, K. Gehmlich, C. Denning, D. Pavlovic, Complex relationship between cardiac fibroblasts and cardiomyocytes in health and disease, J. Am. Heart Assoc. 10 (5) (2021), e019338, https://doi.org/10.1161/JAHA.120.019338.
[76] D. Mayrand, A. Laforce-Lavoie, S. Larochelle, A. Langlois, H. Genest, M. Roy, V. J. Moulin, Angiogenic properties of myofibroblasts isolated from normal human skin wounds, Angiogenesis 15 (2) (2012) 199–212, https://doi.org/10.1007/s10456-012-9253-5.